Electronic Supplementary Information

Unveiling the orientation and dynamics of enzymes in unstructured artificial compartments of Metal-Organic Frameworks (MOFs)

Yanxiong Pan,*[a] Qiaobin Li,[b] Wei Liu,[a] Zoe Armstrong,[b] Austin MacRae,[b] Li Feng,[b] Charles McNeff,[b] Pinjing Zhao,[b] Hui Li,*[c] and Zhongyu Yang*[b]

a. State Key Laboratory of Polymer Physics and Chemistry, Changchun Institute of Applied Chemistry, Chinese Academy of Sciences, Changchun, 130022, China

b. Department of Chemistry and Biochemistry, North Dakota State University, Fargo, ND, 58108 U.S.A.

c. Department of Plant Sciences, North Dakota State University, Fargo, ND, 58108 U.S.A.

Table of Contents

Experimental Procedures

1. One-pot synthesis of aq-ZIF/lys composites in water

To prepare for the aq-ZIF/lys co-crystals, 40 µL lys (16.5 mg/mL) was mixed with 2-methylimidazole (20 mL, 160 mM) and Zinc acetate (20 mL, 40 mM) in water. The obtained mixture was vigorously stirred for 1 min, sonicated for another minute, and incubated at ambient temperature for 24 hr. The products were washed with PBS buffer (pH 7.4) for three times via sonication and centrifugation (10,000 rpm for 10 mins each time); the obtained pellets were dispersed in 800 µL PBS buffer at 4 °C for storage. The spin labeled aq-ZIF/T4L composites were prepared similarly.

2. Transmission Electron Microscopy (TEM)

Copper TEM grids (300-mesh, formvar-carbon coated, Electron Microscopy Sciences, Hatfield, Pennsylvania, USA) were prepared by applying a ~5 µL drop of sample and allowing it to stand for 30 seconds, wicking off the liquid with torn filter paper, then allowing the grids to air dry. After the grids were dried, images were obtained using a JEOL JEM-2100 LaB6 transmission electron microscope (JEOL USA, Peabody, Massachusetts) running at 200 kV.

3. Powder X-ray Diffraction (PXRD)

Powder XRD experiment was performed on Single Crystal Bruker's Diffractometer, Apex 2 Duo with Cu IµS X-ray source. Detector resolution was change to 1024 x 1024 pixels. Data collection strategy is shown on the table below. Images were unwrapped, converted, and integrated with Apex 3 v. 2017.3-0. The final phase analyzes was performed on PAnalytical X'Pert HighScore software.

Table S1. PXRD Data Collection Strategy

Run	Distance [nm]	2-theta [°]	Omega [°]	Chi[°]	Time [sec]
Phi 360	150.000	-12.000	174.000	54.720	180.00
Phi 360	150.000	-24.000	168.000	54.720	180.00
Phi 360	150.000	-36.000	162.000	54.720	180.00
Phi 360	150.000	-48.000	156.000	54.720	180.00
Phi 360	150.000	-60.000	150.000	54.720	180.00

4. Thermogravimetric analysis (TGA)

TGA was measured using a Thermogravimetric Analyzer (TGA), TA Instruments Q500. Each sample was measured between 30 °C to 900 °C at a heating rate of 10 °C/min under a 40 mL/min nitrogen flow.

5. Nitrogen absorption experiments

The porosity and pore size distribution of particles were measured by means of N_2 porosimetry at 77 K (Autosorb-iQ, Quantachrome, Boynton Beach, FL) as described in our recent work.[1] Before the measurement, the char sample was outgassed at 493 K under vacuum. The specific SA of char was calculated by the 11-point Brunauer−Emmett−Teller (BET) method. The micro- and meso-porosities and pore size distributions of char were determined by quenched solid density functional theory (QSDFT) from the N_2 adsorption isotherm at 77 K. QSDFT is a state-of-the-art DFT method for pore size analysis that takes into account the effects of surface roughness and heterogeneity.[2]

Volumetric N_2 porosimetry at 77 K are in widespread use for determination of the pore-size distribution and the BET (Brunauer, Emmett and Teller) surface area of porous materials. N_2 diffusion in micropores at 77 K is kinetically retarded at a relatively low partial pressure.[3, 4] The Autosorb-iQ instrument (Quantachrome, FL) available in our institute typically takes a few days to reach the equilibrium on just one point of adsorption at a low partial pressure. Desorption takes even longer in the low partial pressure region. This presented a serious practical barrier on a shared instrument. Therefore, only a few points were obtained in the low-pressure region. However, the focus of this study is the change of porosity of the crystal upon hL trapping instead of the absolute value of porosity (Figure 2C). The few missing points in the low-pressure region do not change the general trend of porosity. Furthermore, the density functional theory (QSDFT) used for porosity characterization in this study is able to improve the microporosity determination based on N2 porosimetry measurements.[5]

6. Zeta potential:

The zeta potential of the involved bmZIF/lys composites were measured in water using a Nano ZS Zetasizer (Malvern Instrument Ltd.). Specifically, ~20 µL sample dispersed in MeOH was washed with DD water for three times via centrifugation (15,000 rpm) for three times. Then, ~ 10 µL composite was dispersed in 1 mL water and loaded into a disposable folded capillary cell, one at a time, followed by data acquisition. All experiments were conducted at 25 °C. Each sample was repeated for three times to obtain the uncertainty.

7. Lysozyme preparation and characterization

As described previously,[1] the activity assay was conducted using the kit provided by Sigma-Aldrich (Micrococcus lysodeikticus cells, ATCC No. 4698, M3770). Briefly, 10 mg of cells was suspended in 100 mL 66 mM potassium phosphate Buffer. Then, ~ 40 µL 1 µM protein was added into 1 mL of substrates. The active protein degrades the cell walls, which was reflected by the reduction in the optical density at 450 nm.

Mutants of 44C, 65C, 72C, 118C, 131C, and 151C were prepared as described before.[6] Briefly, the mutants were generated by QuikChange site-directed mutagenesis of the pET11a-T4L genetic construct containing the pseudo-wild-type mutations C54T and C97A,[7, 8] followed with verification of each mutation by DNA sequencing.[9] These mutants of T4L were expressed, purified, and then desalted into a buffer suitable for spin labeling (containing 50 mM MOPS and 25 mM NaCl at pH 6.8).[7] The desalted protein mutants were then reacted with a 10 fold molar excess of S-(2,2,5,5-tetramethyl-2,5-dihydro-1H-pyrrol-3-yl) methylmethanesulfonothioate (MTSL, Toronto Research Chemicals, Inc., Toronto) 4°C overnight (yielding R1). Excess MTSL was removed using the Amicon spin concentrator (Millipore, 10,000 MWCO, 50 mL). The spin labeled protein mutants were stored at -20 °C for further use.

The purity of the expressed mutants was confirmed with gel-electrophoresis. As shown in Figure S1, a major band at ~18.7 kDa is consistent with the molecular weight of T4L, while the minor band at ~37 kDa is caused by partial dimerization of the mutant. Besides these two peaks, no other band is visible.

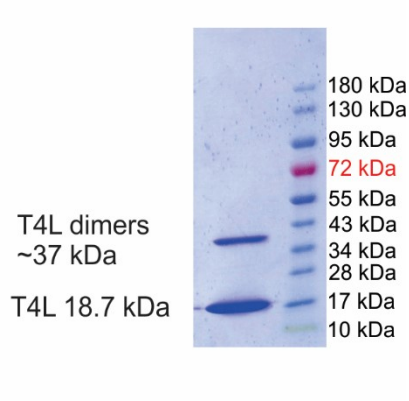

Figure S1. Gel-electrophoresis of the expressed mutants of T4L. Only one mutant (151R1) is shown since all mutants show identical bands.

The secondary structure of 3 representative mutants was confirmed with Circular Dichroism (CD) and shown in Figure S2. As compared to the wildtype protein, all mutants show identical CD spectra, indicating the mutations did not influence the secondary structure of the protein.

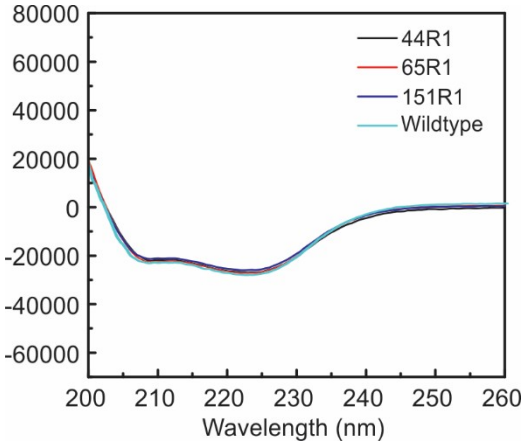

Figure S2. CD spectra of the involved mutants and the wildtype T4L.

All mutants were also confirmed to be functionally active with the same commercial activity kit (Micrococcus lysodeikticus, ATCC No. 4698, Sigma-Aldrich) as described above wherein the bacterial cell walls were mixed with lysozyme and the optical density at 450 nm (OD450) was monitored. A drop in OD450 indicates cell wall breakage by functional lysozyme. As shown in Figure S3, the three mutants show a similar capability to drop the OD450. The "control" was water which does not influence the OD450.

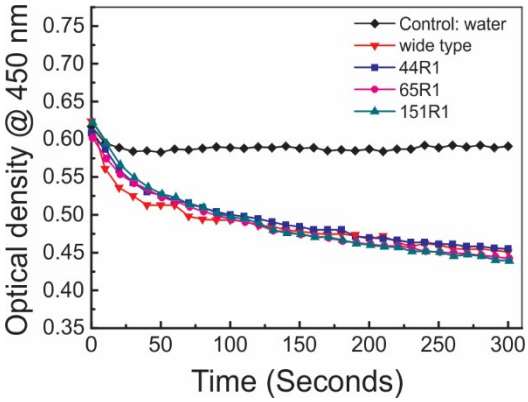

Figure S3. The activity assay of three mutants and the wildtype protein of T4L. A drop in OD450 was observed for all protein samples. The "control" was acquired by mixing water with the bacterial cell walls.

8. Electron Paramagnetic Resonance (EPR) spectroscopy

For EPR measurements, composites samples were transferred into a borosilicate capillary tube (0.70 mm i.d./1.00 mm o.d.; Wilmad Labglass, Inc.). A Varian E-109 spectrometer equipped with a cavity resonator was used for the acquisition. All continuous wave (CW) EPR spectra were obtained with an observe power of 200 μW, a modulation frequency of 100 kHz, and a modulation amplitude of 1.0 G.

9. EPR spectral analysis

The CW EPR spectra were fit using the software developed by Dr. Altenbach and Prof. Hubbell at UCLA (http://www.biochemistry.ucla.edu/biochem/Faculty/Hubbell/). This program was essentially the MOMD model of the NSLS program established by Freed and co-workers.[10] In our case, the MOMD model includes three coordinate frames to describe the internal motion of the nitroxide spin label in a hybrid. First, the molecular frame which is consistent with the magnetic tensor (g- and hyperfine-tensor) frame (x_M, y_M, z_M). The z_M is defined as to be along with the nitroxide p orbital; the x_M is parallel with the NO bond axis; the y_M follows a right-handed coordinate system. Second, the principle frame of the rotational diffusion tensor (x_R, y_R, z_R), which usually deviate from the molecular frame. Although in principle three Euler angles are required to correlate the two frames, experiences from spectral simulations indicated that only the β_D, the angle between z_R and z_M (Figure S4), is important for simulations. Third, the coordinate frame describing the diffusion of the spin label on the attached protein, the director frame, (x_D, y_D, z_D). A good approximation/simplification is to allow the spin label to rotate/move freely within a cone (Figure S4). This also leads to simplifying the rotational diffusion tensor R, wherein the axial symmetry can be assumed. The angle between z_D and z_R is defined as θ.

According to Budil et al,[10] a restoring (ordering) potential (U) is appropriate to describe the extent of spatial constrains of the spin label within the "cone". The restoring potential $U(\theta) = -1/2k_BTc_0^2\,(3\cos^2\theta - 1) + \text{H.O.T.}$, where c_0^2 is a scaling coefficient and H.O.T. represents higher order terms as defined in the literature.[10] In our simulations, only the dominant term and the first H.O.T. term was involved, the coefficients of which are C_{20} and C_{22} in our simulations, respectively.

For describing the nitroxide side chains on a protein to the above ordering potential, the director frame is fixed. The existence of the restoring potential results in an anisotropic motion and can be characterized by the order parameter $S = -1/2\langle(3\cos^2\theta - 1)\rangle$, where the brackets indicate spatial average. For an individual protein molecule, z_D forms an angle ψ with respect to the external magnetic field. To obtain the final spectrum corresponding to an isotropic distribution of protein orientations, the spectra are summed over ψ.

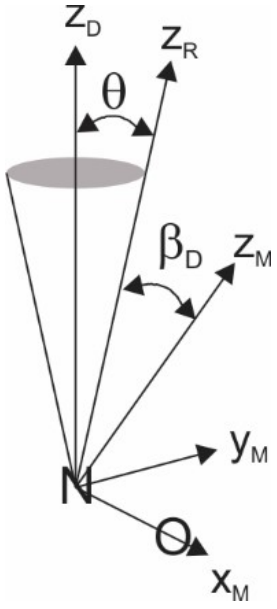

Figure S4. Definition of the three coordinate systems (ZD, ZR, and ZM) related to the MOMD model used in our simulations.

The starting values for the diagonal values of the g and hyperfine (A) tensors were: g_{xx} = 2.0078, g_{yy} = 2.0058, g_{zz} = 2.0022 and A_{xx} = 6.2 G, A_{yy} = 5.9 G, A_{zz} = 37.0 G.[11] The rotational correlation rates were described by the rotational diffusion tensor. For simplicity, symmetric motion is assumed and this assumption was found to provide reasonably good fit to the data. The mean rotational diffusion constant is defined as R.[10] The average effective correlation time is computed as $\tau_c = 1/(6<R>)$. Spatial ordering

of the diffusion tensor is accounted for by the order parameters, S_{20} and S_{22}, computed from the C_{20} and C_{22} coefficients of the ordering potential which was varied in fitting.[10] The tilt of the diffusion tensor with respect to the molecular axis of the nitroxide is specified by the Euler angles (α_D, β_D, γ_D). For axially symmetric motion ($R_x = R_y$), only β_D and γ_D need be specified. For z-axis anisotropic motion, the diffusion tilt was fixed at $\beta_D = 36°$, $\gamma_D = 0°$.[12]

The Rs, C_{20}, and C_{22} parameters were varied in the simulations to fit the selected data. During fitting, the center peak area was weighted as 50% of the rest of the spectrum, in order to better fit the low and high field regions, which are more sensitive to the rate and order. After a good fit was obtained, the diagonal elements of the A and g tensors were varied slightly to obtain the best fit. The fitting parameters are listed in Table S2.

Table S2. Best Fitting Parameters for each labelled mutant.

	$R_{z,\,im}$[b]	$R_{z,m}$[b]	$R_{2,im}$	$R_{2,m}$	$C_{20,im}$	$C_{22,im}$	$C_{20,m}$	$C_{22,m}$	$Population_m$	χ^2
44R1	6.10	7.81	1.06	-1.39	44	-43	-13	3.28	42%	1.51e-5
44R1_u[a]	6.12	8.16	0.01	-0.57	39	-39	-18	0.04	32%	3.86e-5
65R1	6.02	7.91	1.28	-1.03	44	-42	-20	2.0	53%	2.62e-5
65R1_u	6.18	8.07	1.06	-0.47	39	-39	-18	0.78	29%	1.70e-5
72R1	6.02	7.78	1.03	-0.9	44	-43	-20	3.67	56%	2.93e-5
72R1_u	6.20	8.20	-0.48	-0.35	27	-27	-16	2.6	21%	5.93e-5
118R1	6.06	8.23	1.01	-0.2	47	-46	-19	2.76	25%	2.06e-5
118R1_u	6.23	8.53	0.41	-1.19	38	-42	-18	0.22	18%	3.30e-5
131R1	6.04	8.11	0.97	-0.25	43	-45	-18	2.6	46%	1.99e-5
131R1_u	6.23	8.22	0.93	-0.48	40	-40	-18	0.42	17%	1.99e-5
151R1	6.03	8.10	0.74	-0.26	40	-45	-18	2.89	38%	5.85e-5
151R1_u	6.20	8.50	-2.64	0.24	16	-17	2.2	3.6	13%	5.65e-5

[a] Subscript "u" indicates the labelled mutant treated with 6 M urea. Shades are included to improve the clarity of the table. [b] Subscripts "im" and "m" indicate the immobile and mobile components, respectively, utilized in the simulations.

10. Urea unfolds the exposed portion of the trapped protein

The composites was mixed with 6 M urea and incubated at ambient temperature in an Eppendorf tube (1.5 mL). At different time point an aliquot of the mixture was taken for an EPR test. As is evident from the data, 16-20 hr incubation is sufficient for the unfolding to complete.[1] Therefore, for all Urea esxperiments, the incubation time was 20 hr.

11. Using EPR to estimate the amount of encapsulated proteins.

A calibration curve was established by plotting the integrated intensity of CW EPR spectra as a function of standard protein concentration. Our protein concentration range in this case is 28.5 to 920 μM. A linear correlation can be seen from Figure S5. Using this curve, we back calculated the concentration of each of our spin labeled mutant.

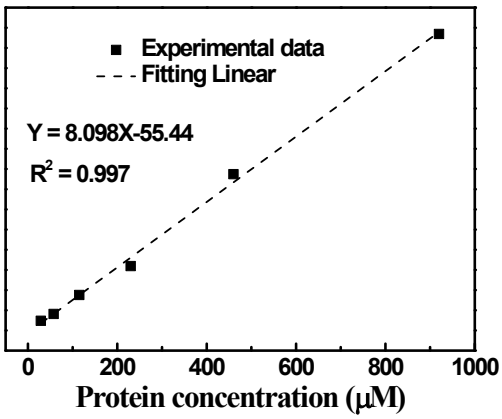

Figure S5. The calibration curve to estimate the amount of trapped protein in ZIF8. The y-axis is the integrated spectral density while the x-axis is the concentration of known protein.

12. Aromatic residues in T4L.

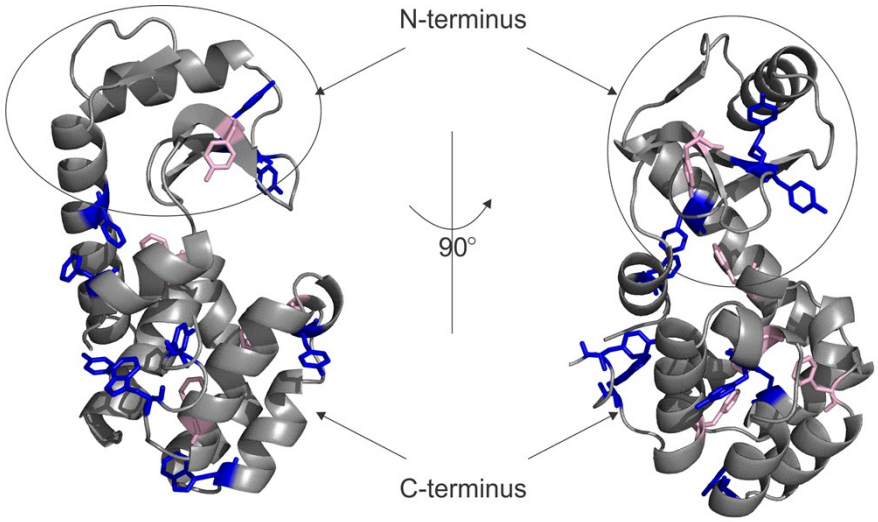

Figure S6. Aromatic residues of T4L from two views. There are more solvent exposable aromatic residues (blue sticks) in the C-terminus than in the N-terminus. Buried aromatic residues are shown in light pink sticks.

References

1. Y. Pan, H. Li, J. Farmakes, F. Xiao, B. Chen, S. Ma and Z. Yang, *J. Am. Chem. Soc.*, 2018, **140**, 16032-16036.
2. A. V. Neimark, Y. Lin, P. I. Ravikovitch and M. Thommes, *Carbon*, 2009, **47**, 1617-1628.
3. J. C. Echeverria, M. T. Morera, C. Mazkiaran and J. J. Garrido, *Euro. J. Soil Sci.*, 2008, **50**, 497-503.
4. J. Garrido, A. Linares-Solano, J. M. Martin-Martinez, M. Molina-Sabio, F. Rodriguez-Reinoso and R. Torregrosa, *Langmuir*, 1987, **3**, 76-81.
5. Quantachrome. Quantachrome Instruments. Quenched solid state functional theory (QSDFT) for pore size analysis of disordered carbon, <https://www.azom.com/article.aspx?ArticleID=5191>

(access May 2017). , DOI: https://www.azom.com/article.aspx?ArticleID=5191 (access May 2017).).
6. Z. Yang, G. Jiménez-Osés, C. J. López, M. D. Bridges, K. N. Houk and W. L. Hubbell, *J. Am. Chem. Soc.*, 2014, **136**, 15356-15365.
7. C. J. López, M. R. Fleissner, Z. Guo, A. K. Kusnetzow and W. L. Hubbell, *Prot. Sci.*, 2009, **18**, 1637-1652.
8. M. R. Fleissner, E. M. Brustad, T. Kálai, C. Altenbach, D. Cascio, F. B. Peters, K. Hideg, S. Peuker, P. G. Schultz and W. L. Hubbell, *Proc. Natl. Acad. Sci.*, 2009, **106**, 21637-21642.
9. M. Matsumura, J. A. Wozniak, D. P. Sun and B. W. Matthews, *J. Biol. Chem.*, 1989, **264**, 16059-16066.
10. D. E. Budil, S. Lee, S. Saxena and J. H. Freed, *J. Magn. Reson. A*, 1996, **120**, 155-189.
11. A. K. Kusnetzow, C. Altenbach and W. L. Hubbell, *Biochemistry*, 2006, **45**, 5538-5550.
12. L. Columbus, T. Kálai, J. Jekö, K. Hideg and W. L. Hubbell, *Biochemistry*, 2001, **40**, 3828-3846.